ACADEMIA ROMÂNĂ
Revue Roumaine de Chimie
http://web.icf.ro/rrch/

Rev. Roum. Chim.,
2018, *63*(7-8), 673-684

Dedicated to Professor Bogdan C. Simionescu on the occasion of his 70th anniversary

INVESTIGATION OF A SELF-ASSEMBLED NANOGEL STRUCTURE BEARING SPIROACETAL MOIETIES AND CHOLESTEROL AS LOW MOLECULAR MASS GELATOR

Aurica P. CHIRIAC,* Alina G. RUSU, Nita TUDORACHI, Loredana E. NITA, Alina DIACONU, Daniela RUSU, Iordana NEAMTU, Mihai ASANDULESA and Vlad Mihai CHIRIAC

"Petru Poni" Institute of Macromolecular Chemistry, 41-A Grigore Ghica Voda Alley, RO-700487 Iaşi, Roumania

Received July 31, 2017

The research is following the properties of a new nanogel structure (PItAU_Ch) based on poly(itaconic anhydride-co-3,9-divinyl-2,4,8,10-tetraoxaspiro[5.5] undecane) and a low molecular mass gelator, namely cholesterol. The interest is entirely justified as nano-sized gel systems, presenting 3D polymer structures, are considered to be the most effective carriers owing to their dimension and capacity to hold larger amounts of solvent for the incorporation of bioactive compounds, for example. The physicochemical characteristics of the new PItAU_Ch structure are evaluated in terms of their thermal stability, spectroscopic and dielectric properties, to have useful information for the subsequent use of these nanogels.

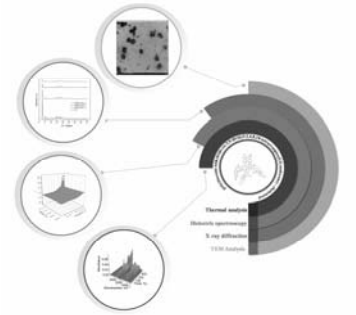

INTRODUCTION

The interest in using low molecular mass gelators (LMGs) is already well known, as long as they can assure supramolecular self-assembly, generation of three-dimensional continuous networks, even at low concentration, and build thermo-reversible networks like aggregates.[1] More than that, by choosing the appropriate chemical structure of the LMG, it is possible by precise variations of the ratio between the components to control the properties and morphology of the new network, and thus, to tune the materials functionality in order to respond and to match specific applications in the medical science or for the template material synthesis. The functional network materials present supramolecular architecture resulted through the self-organization of the interconnecting sites.

Cholesterol is one of the most versatile compounds that forms supramolecular aggregates[2,3] and is used for the design and preparation of liquid crystals,[4-6] gels[7-11] and Langmuir-Blodgett (LB) films.[12,13] The cholesterol-based gelators induce molecular aggregation and directed/targeted self-association through non-hydrogen bonds owing to their hydrophobic and rigid skeleton, sterogenic centers, and capacity to form aggregates via van der Waals interactions.[10, 13-17]

In our previous investigations it was presented the synthesis of some macromolecular compounds with spiroacetal moieties in the structure, which bring specific conformational framework, acidic pH sensitivity, and capacity for complexation to

* Corresponding author: achiriac1@yahoo.com; tel. +40232217454; fax. +40232211299

the etheric oxygen by means of hydrogen or coordinate bonds, dynamic changes of the stereochemistry and anomeric effect performed once the pH is increasing.[18-20] One of this kind of structures is poly(itaconic anhydride–co–3,9-divinyl-2,4,8,10-tetraoxaspiro[5.5] undecane) (PITAU), a macromolecular compound capable of network formation, which has between other properties amphilicity, good oxidative and thermal stability, good films former, acidic pH sensitivity, binding characteristics, biodegradability, biocompatibility, and gel formation capacity.[21-23] Owing to the anhydride ring presence, the copolymer can be as well modified through suitable reactions, and in this context we investigated the possibility of building a new nano-network by using cholesterol as low molecular mass gelator. Aspects concerning the synthesis of the network based on poly(itaconic anhydride–co–3,9-divinyl-2,4,8,10-tetraoxaspiro[5.5] undecane) copolymer and cholesterol (Ch) (PItAU_Ch) were already presented.[24-26]

In this study, supplementary data are presented concerning the functional and structural characteristics of PItAU_Ch, investigations that will allow exploitation of this network structure in the future. Thus, there were evaluated the physicochemical characteristics of PItAU_Ch in terms of thermal stability, microscopic, spectroscopic and dielectric properties, in order to have useful information for the subsequent specific use of these compounds.

RESULTS AND DISCUSSION

The schematized structure of the new PItAU_Ch 3D network is illustrated in Figure 1. The chemical composition and the environmental sensitivity of PItAU_Ch nanogel have already been established. [27] In the present investigation, it is confirmed the coupling of Ch through covalent bonds to the PItAU copolymer by opening the itaconic anhydride cycle, evidenced by the thermal properties of the new network, and also by other properties brought to the PItAU network system after the self-assembly process generated by the Ch presence.

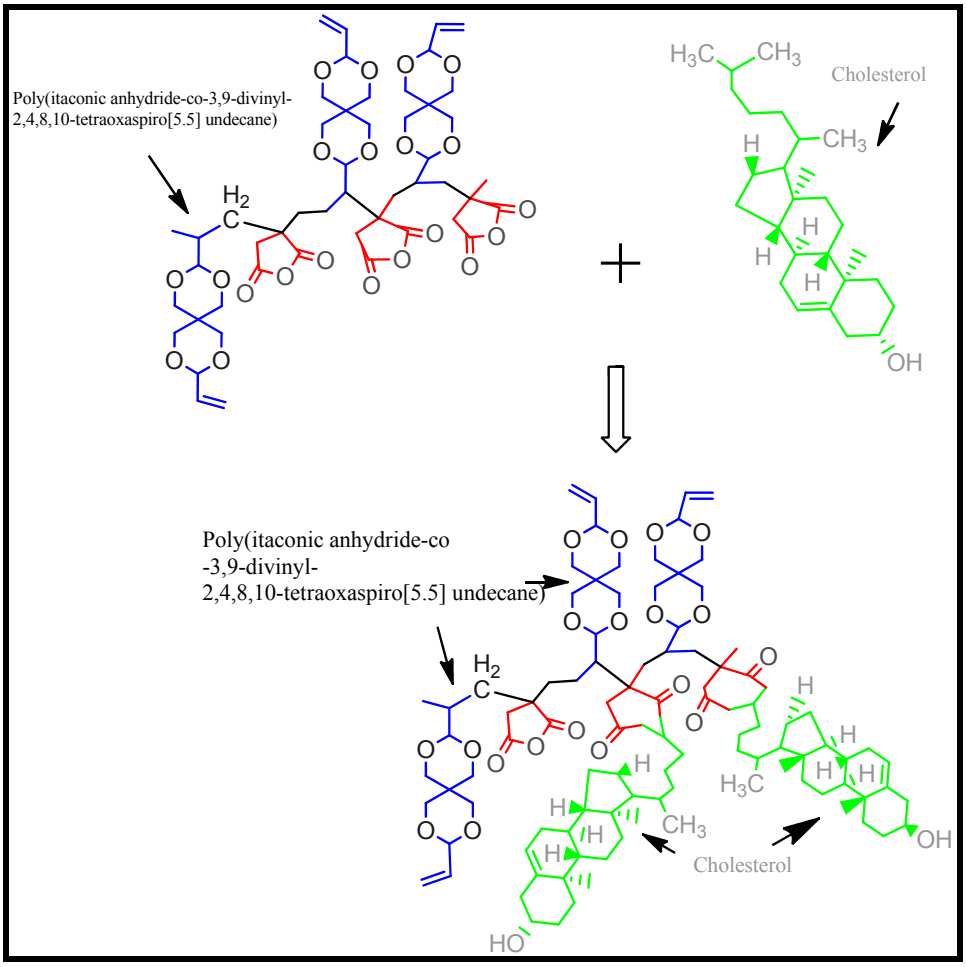

Fig. 1 – Idealized schematic representation of the PITAU_Ch 3D structure.

1. The thermal analysis of the PItAU_Ch 3D structures

The thermal behaviour of the PItAU_Ch structure comparative to the PItAU copolymer and Ch investigated by thermogravimetric analysis is illustrated in Fig. 2 and the thermal parameters are presented in Table 1. The TG curves were recorded by measuring the mass losses between 30°C and 650°C, in inert atmosphere (N_2) with a heating rate of 10°C·min^{-1}. The presented thermogravimetric data and the shape of the TG/DTG curves indicate different thermal behaviour for the three structures. The PItAU copolymer exhibits mass losses of approx. 23% in the first stage (T_{onset} = 121°C) mainly due to the elimination of adsorption water and the breakdown of the itaconic anhydride ring with the formation and elimination of CO or CO_2. Increasing the temperature above 300°C generates significant mass losses (over 63%) caused by the breakage of C-C bonds, initiation of recombination or cyclization reactions and elimination of gaseous products formed. On the other hand, the PItAU_Ch sample exhibits a first thermal degradation at a higher temperature (T_{onset} = 138°C) where the mass losses are low (11%), which implies complexation or cross-linking reaction between PItAU and cholesterol. The actual thermal degradation occurs at over 300°C when the C-C bonds are broken and the cyclic or linear aliphatic derivatives are formed, as well as certain carbonyl derivatives that can contribute to massive mass losses. In this process, not only the PItAU structural units are decomposing, but also those of Ch in particular, observation sustained by the thermal degradation of Ch that starts at over 350°C and takes place in a single stage with a total mass loss up to 420°C. Analysing the thermal stability of PItAU_Ch, compared to PItAU, by assessing the temperatures at which mass losses of 10% and 20%, respectively, are recorded, it is found that PItAU_Ch is more thermally stable than PItAU. In the case of PItAU_Ch, the temperature values corresponding to T_{10} and T_{20} are 270°C and 309°C, while for PItAU T_{10} =192°C and T_{20} =274°C. This behaviour is influenced by the Ch compound whose values for T_{10} and T_{20} are much higher (Table 1).

The main gases released by thermal decomposition of PItAU_Ch were analysed with TG-DTA/FTIR/MS system on the temperature interval of 30–650°C. In Fig. 3a, it is shown the 3D FT-IR spectrum of PItAU_Ch sample and it can be noticed that the major release of gases by thermal decomposition takes place between 250 and 450°C (as can be seen in Fig. 2 and from the GS values extracted in Table 2). In this temperature interval, there take place scissions of the itaconic anhydride units, OH functional groups, tetraoxaspiro cycle and C-C bonds which belong to the respective structures.

The FT-IR 2D spectra (Fig. 3b) corresponding to the gases evolved at 380 and 440°C were extracted from the 3D FT-IR spectrum of the samples. The evolved gases were identified on the basis of IR spectra and MS signals available in the spectral libraries of the NIST. [28] In these spectra, it can be seen that characteristic absorption bands are appearing in the regions: 3859-3602, 3252, 2955-2822, 2433- 2355, 2180-2110, 1780-1681, 1552, 1482-1434, 1341-1046, 940-801 and 743-597 cm^{-1}. The absorption band recorded at about 3252 cm^{-1} is attributed to the MCT detector from TGA-IR external module. [29] In Table 2 are presented the main absorption bands belonging to certain classes of gaseous products resulting from the thermal degradation of the PItAU_Ch structure.

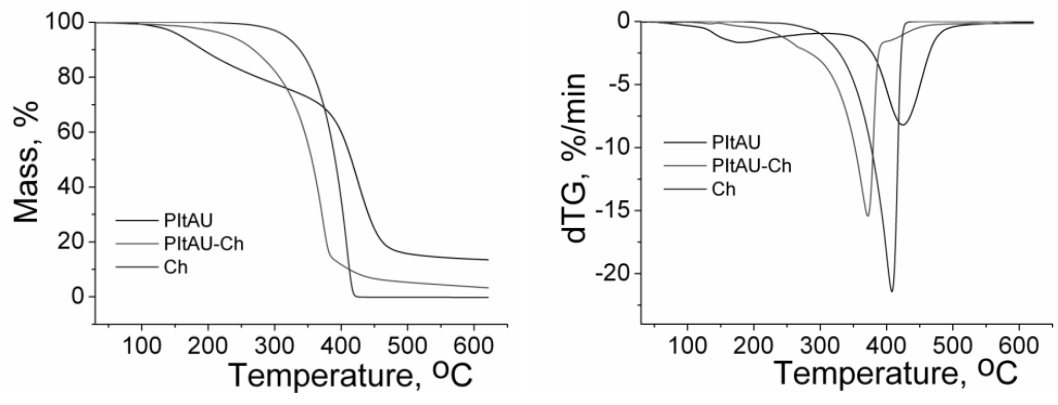

a) b)

Fig. 2 – TG (a) and dTG (b) curves of the studied samples.

Table 1

Thermal parameters obtained by thermogravimetric analysis

Sample	Degradation stage	T_{onset} °C	T_{peak} °C	W %	T_{10} °C	T_{20} °C	GS °C
PItAU	I II residue	121 377	177 425	23.33 63.21 13.46	192	274	
PItAU-Ch	I II III residue	138 338 400	- 374 -	10.93 76.95 9.60 2.52	270	309	380 440
Ch	I residue	363	410	100 -	339	361	

T_{onset} – the temperature at which the thermal degradation starts.
T_{peak} – the temperature at which the degradation rate is maximum.
W – the final mass losses.
T_{10}, T_{20} – the temperatures corresponding to 10 wt.% and 20 wt.% weight losses
GS – the temperature at which the maximum amount of gases was released (from Gram–Schmidt curve).

Table 2

The main IR absorption bands

Wavenumber, cm^{-1}	Functional groups
3602, 3737, 3403, 1046 cm^{-1} 1552 cm^{-1}	νC-OH stretching vibrations δOH deformation vibrations (in water, alcohols, phenols)
2355, 684 cm^{-1}	νC=O (in CO_2)
2180, 2110 cm^{-1}	νC=O (in CO)
2955, 2885, 2822 , 1341, cm^{-1}	νCH, νCH_2, νCH_3 (in aliphatic derivatives)
3031,1681, 1433, 940, 868-743 cm^{-1}	νC=C unsaturated bonds (in aliphatic and aromatic derivatives)
1780, cm^{-1}	νC=O vibrations (in esters, acids, unsaturated aldehydes)
1283, 1137, 1212 cm^{-1}	νCO (in ethers, anhydride)
3252 cm^{-1}	absorption band for MCT detector

The compounds identified by FTIR spectroscopy were also confirmed through mass spectroscopy (Fig. 3c). The MS signals were represented at 385°C when a maximum amount of gases is released. The signals can be associated with the chains scission of PItAU and Ch and some fragmentation or recombination reactions occurring at high temperatures. Pyrolysis of Ch leads to the breakage of the chemical bonds between the aromatic and aliphatic moiety of the chemical structure (position 17 on Ch) resulting polycyclic aromatic hydrocarbons substituted and unsubstituted, such as: phenantrene, methylphenantrene, fluorene, methylfluorene, naphthalene, but also some cyclic or linear aliphatic hydrocarbons (saturated/unsaturated) formed by the pyrolysis of the aliphatic moieties.[30, 31]

Also, the pyrolysis of PItAU structural units led to the formation of other gaseous products by breaking the itaconic anhydride molecules and the tetraoxaspiro undecane cycles, that were revealed by FTIR and MS spectroscopy. [22, 23] The main ionic fragments identified by mass spectroscopy, as a result of the thermal degradation of PItAU_Ch sample, were: water H_2O (m/z 18), carbon dioxide CO_2 (m/z 44), carbon monoxide CO (m/z 28), ethane C_2H_6 (m/z 30), propane C_3H_8 {m/z 44), cyclopropane C_3H_6 (42), butane C_4H_{10} (m/z 58), cyclobutane C_4H_8 (m/z 56), benzene C_6H_6 (m/z 78), cyclohexane C_6H_{12} (m/z 84), phenol C_6H_6O (m/z 96), isoheptane C_7H_{16} (m/z 100), itaconic anhydride $C_5H_4O_3$ (m/z 112), phenantrene $C_{14}H_{10}$ (m/z 178), methyl phenantrene $C_{15}H_{12}$ (m/z 192), hydroxyphenanthrene (phenanthrenol) $C_{14}H_{10}O$ (m/z 194), naphthalene $C_{10}H_8$ (m/z 128), methylnaphthalene $C_{11}H_{10}$ (m/z 142), naphthol $C_{10}H_8O$ (m/z 144), androst-5ene-3-ol $C_{19}H_{30}O$ (m/z 274).

2. Scanning Electron Microscopy

In order to visualize the shape and the morphological aspects of the synthesised nanogels, observations and structural studies were made by scanning electron microscopy (SEM). At the same

time, the EDAX microanalysis was performed in order to confirm the composition of the new network structure, respectively the addition of Ch covalent bonded to PItAU copolymer. The internal nanostructure, organized in small clusters as result of the Ch presence, and the reports concerning the composition of the visualised structures are presented in Table 3. Clear differences in the morphological aspect, as well in the composition are registered for the studied compounds, namely PItAU, PItAU_Ch (1:1) and PItAU_Ch (2:1). Thus, the presence of cholesterol is reflected in a more laced morphology that emphasizes its supramolecular organizational capacity and the formation of self-assembled structures.

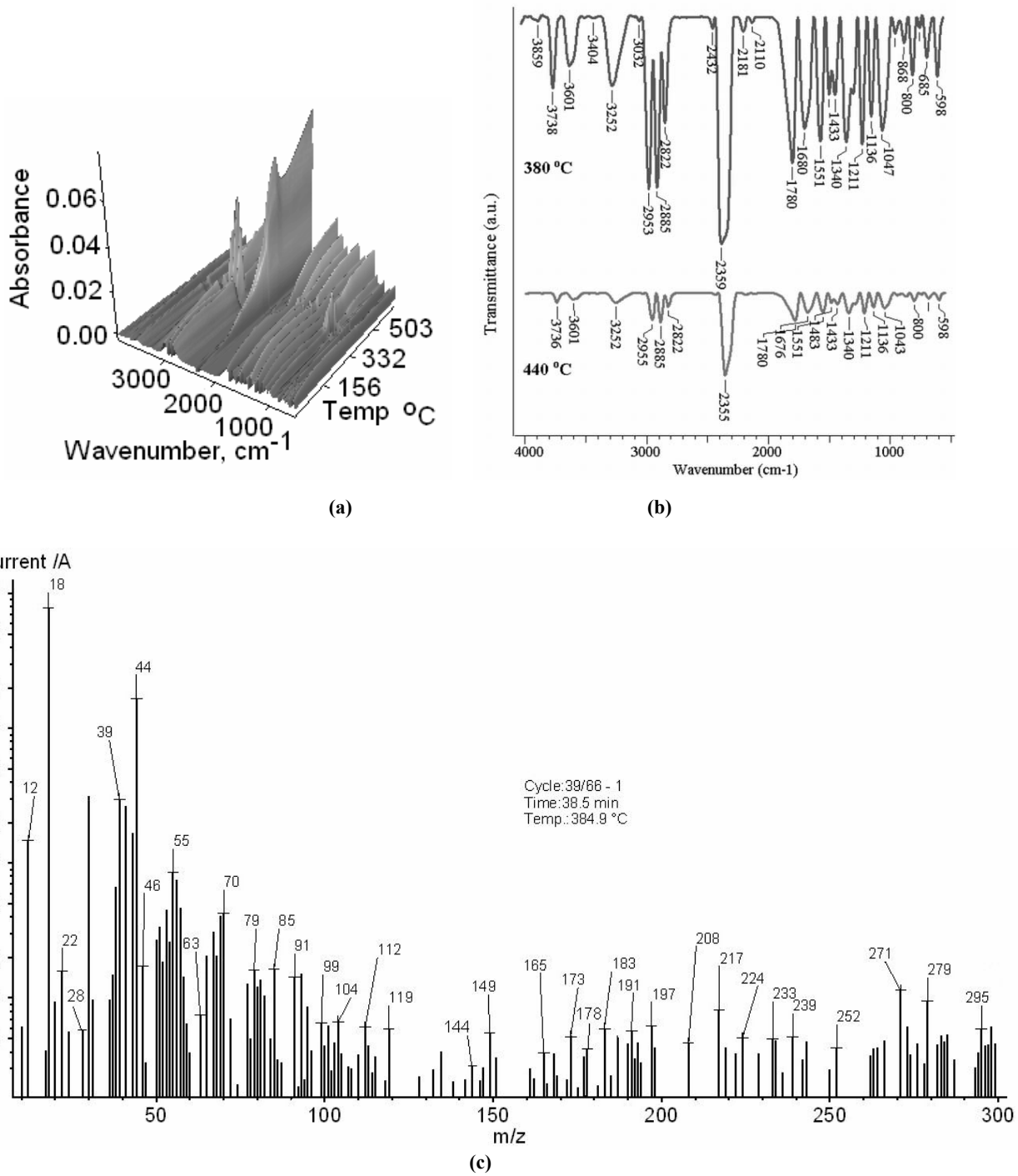

Fig. 3 – FTIR 3D spectrum of the PItAU_Ch sample (a), FTIR 2D spectra of the evolved gases from the thermal decomposition of the PItAU_Ch sample at 380°C and 440°C (b), and MS graphic of the evolved gases at the temperature of 385°C.

Table 3

The percentage of the elements identified in the composition of the studied compounds by EDAX analysis

Sample	Detected constitutive elements	Selected image from the analysed sample
PItAU	**Carbon = 64.16 % Wt (70.29 percentage)** **Nitrogen = 01.98 % Wt (01.86 percentage)** **Oxygen = 33.86 % Wt (27.85 percentage)**	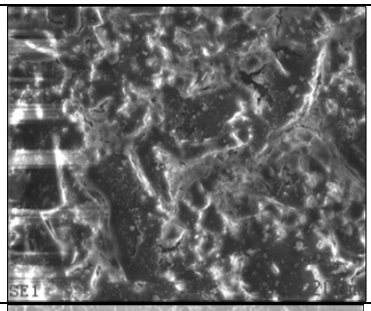
PItAU_Ch (2:1)	**Carbon = 68.76 % Wt (74.25 percentage)** **Nitrogen = 03.68 % Wt (03.41 percentage)** **Oxygen = 27.56 % Wt (22.34 percentage)**	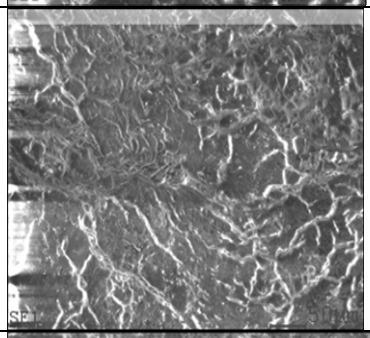
PItAU_Ch (1:1)	**Carbon = 74.57 % Wt (79.25 percentage)** **Nitrogen = 04.03 % Wt (03.67 percentage)** **Oxygen = 21.40 % Wt (17.07 percentage)**	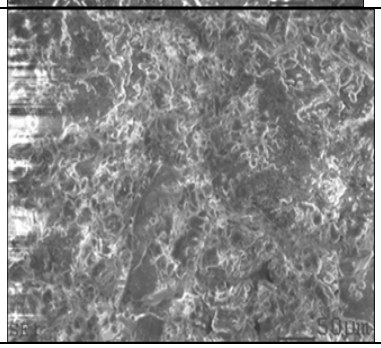

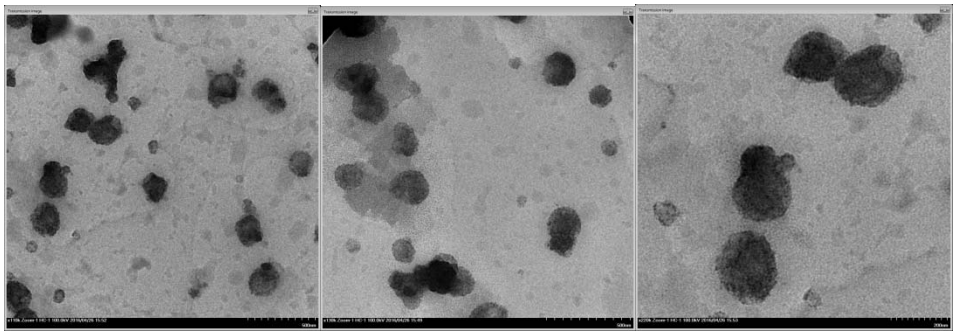

(a) **(b)** **(c)**

Fig. 4 – TEM images for PITAU/Ch samples synthesised in ratio of 4/1 (a), 2/1(b), and (c) 1/1.

3. Transmission Electron Microscopy

Typical transmission electron microscopy (TEM) representations of the PItAU_Ch nanogels in direct correlation with the synthesis procedure, namely the Ch content, are shown in Fig. 4 a-c. Thus, the morphology of the nanogels is confirmed via TEM. The images clearly demonstrate the connection between the Ch content and the cholesterol capacity to induce self-assembly processes as the synthesised nanogels present well-defined spherical morphology. It is known that Ch

is used as hydrophobic moiety to form nanogel structures with amphiphilic copolymers which can respond to the hydrophilic/hydrophobic balance. In the case of the new structure, Ch, which is covalently bonded to PItAU, determines as well the crosslinking of the macromolecular chains and generates the three-dimensional network formation. Growth of the Ch content induces the increasing of the intramolecular physical bonds, phenomenon reflected by the reduction of the nanogel particle size, as can be seen in Fig. 4. This aspect is in good agreement with the data resulted from the dynamic light scattering investigation.[27]

4. X-ray diffraction analysis

X-ray diffraction is generally used to determine whether the materials are crystalline or amorphous. Normally, PItAU presents an amorphous structure as opposed to cholesterol, which, as mentioned in the literature, presents peaks at 3.80, 4.89, 5.47, 5.90, 6.30, and 17.30Å. [32, 33]

As it is illustrated in Figure 5, the peaks at 2.80, 5.47, 6.30, and 17.30Å which are found in the cholesterol diffractogram are also noticed in the PItAU_Ch complex spectrum attesting the presence of Ch covalent bonded. Nevertheless, the intensity of PItAU_Ch peaks is lower than that of Ch, which is in good agreement with the Ch content from the network gel structure.

5. Circular dichroism analysis

CD, as a non-destructive and powerful technique, is able to elucidate the structure in solution of the compounds that encompass small chiral molecules.[34] As mentioned in the literature, liquid crystal molecules based on cholesterol possess a high degree of molecular chirality (Ch contains 8 chiral centres) and can form helical structures via molecular assembly, which were put into evidence by CD spectra.[35, 36]

The CD curves enable as well to evaluate the structural changes which intervened through the presence of small chiral molecules. Figure 6 illustrates the circular dichroism spectra of Ch and PItAU_Ch self-assembled structure. The clear CD spectrum corresponds to Ch solution, and instead, the PItAU_Ch spectrum, even if it has the same shape as that of Ch, presents a more reduced signal. This diminution is primarily due to the reduced content of Ch, and at the same time to the restrictions in orientation owing to the presence of the spiroacetal structure that functions as a crosslinker and which offers a limited and specific conformational framework for the copolymers.[37]

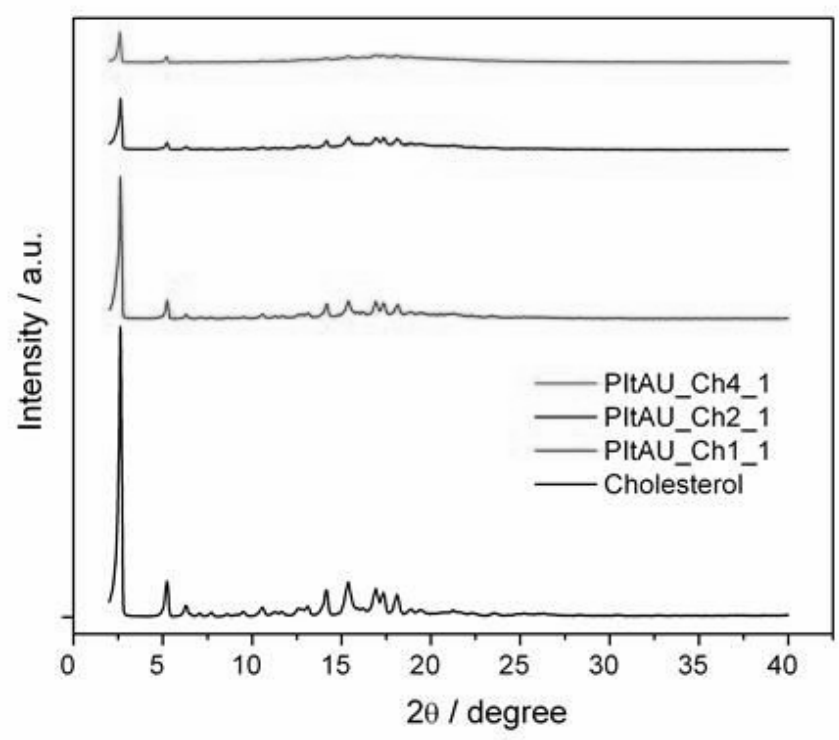

Fig. 5 – X ray diffractograms of Ch and PITAU/Ch sample with copolymer and Ch found in ratio of 1/1, 2/1 and 4/1.

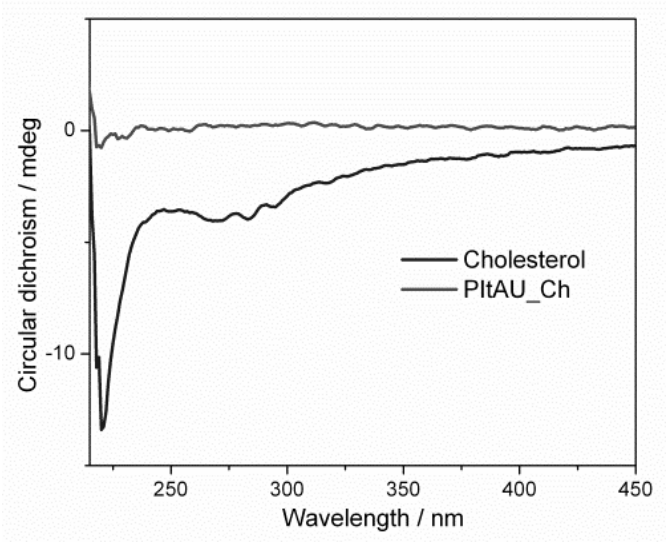

Fig. 6 – The circular dichroism spectra of Ch and PItAU_Ch network (PItAU/Ch in ratio of 2/1).

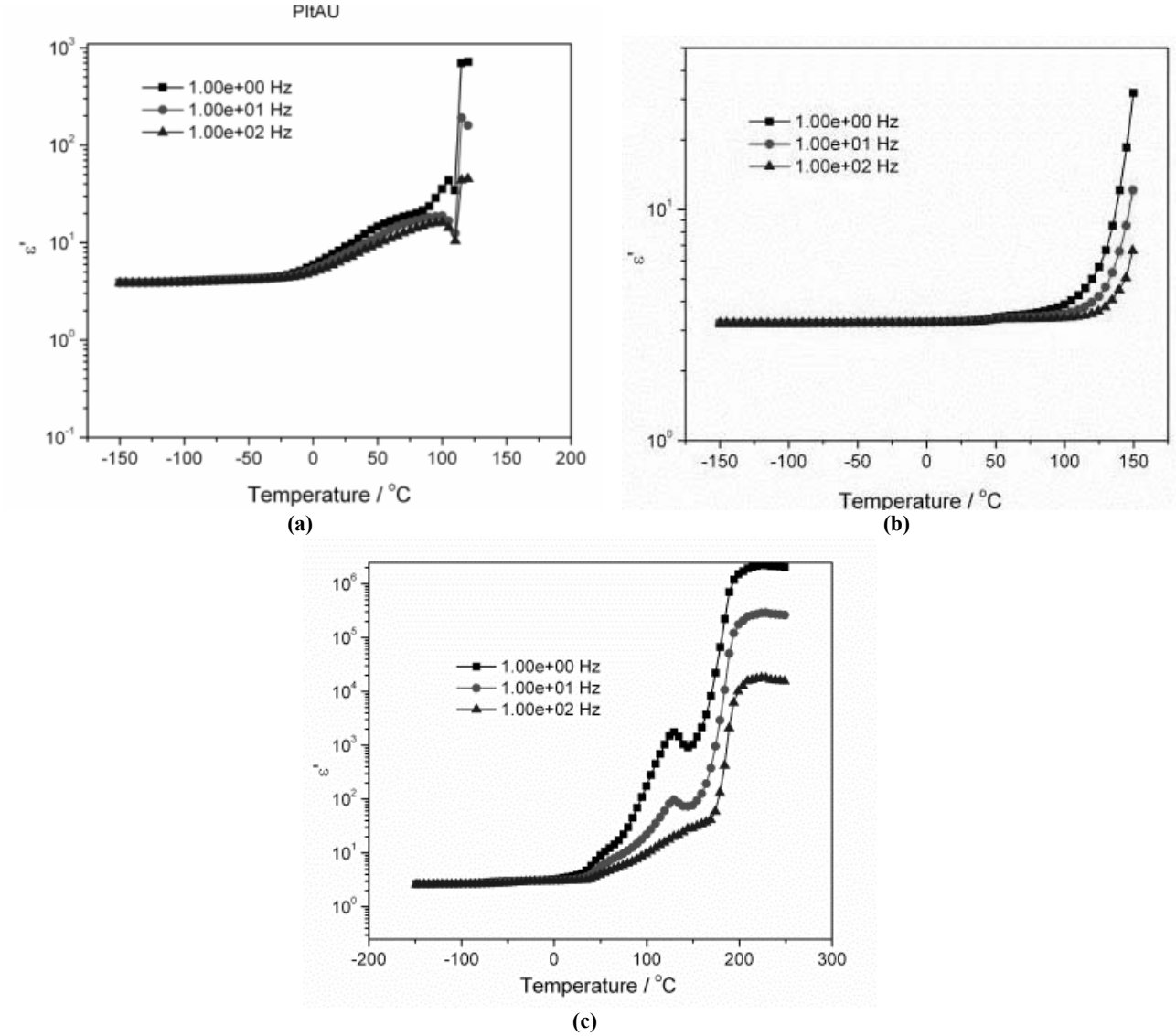

Fig. 7 – Logarithmic plot of the dielectric constant (ε') for PItAU (a), Ch (b) and PItAU_Ch (1:1 (c) as a function of temperature and specified frequencies.

6. Dielectric spectroscopy

The phenomena of electrical polarization of a macromolecular compound are closely related to its structure, the presence of functional groups capable to respond to the electric field that acts upon it, meanwhile the dipole orientation rate is closely related to inter- and intramolecular interactions. At the same time, the orientation of the dipoles occurs in a wide range of frequencies depending on the ease with which the dipoles are directed under the action of the electric field. [38] In this context, it is expected that the covalent coupling of Ch on the PItAU structure to modify the electronic polarization (achieved by a slight shift of the electron cloud of each atom relative to the nucleus) and the orientation polarization (occurring when some molecular clusters exhibit a permanent, randomly oriented electric moment in space, but which will orient in the field direction) of the new structure compared with the starting/original PItAU copolymer.

Figure 7 illustrates the dependence of the dielectric constant on temperature for the studied samples, which is determined by the induced dipoles and the dipolar orientation.

As it can be observed, clear changes occur between the evolution of the dielectric constant values for the Ch, PItAU copolymer and that of the new PItAU_Ch structure. Thus, the dielectric constant constantly increases from 40°C attesting the opening of the itaconic anhydride cycle with formation of dipoles capable of orientation in the field. At the same time, the dielectric constant presents a slight decrease with the increasing of frequency owing to the lag of polarizable units that could orientate in the direction of the alternative electric field at higher frequencies.

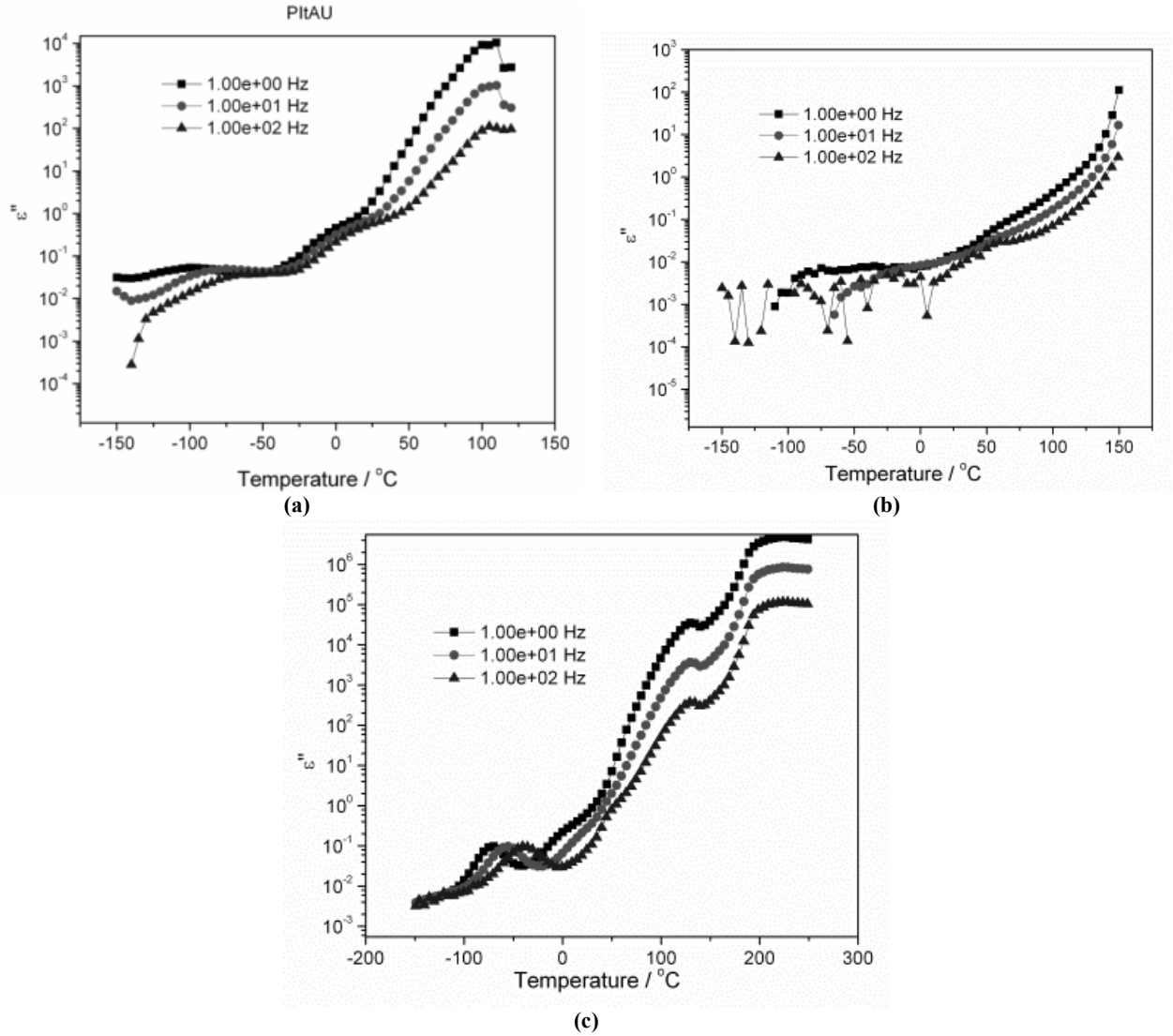

Fig. 8 – Logarithmic plot of the dielectric loss (ε'') of PItAU (a), Ch (b) and PItAU_Ch in ratio of 1/1 (c) as a function of temperature and specified frequencies.

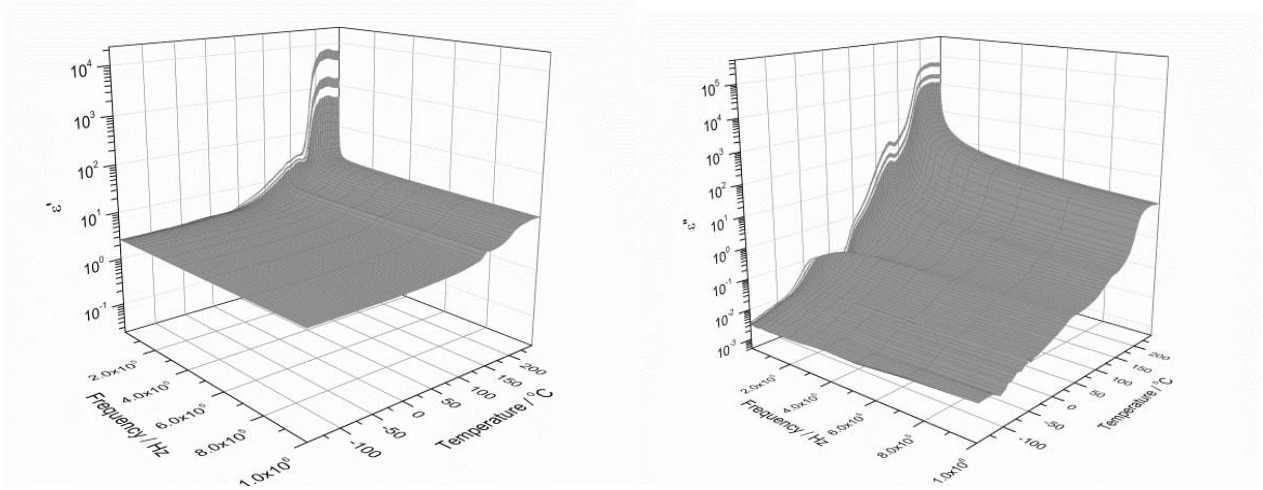

Fig. 9 – Dielectric permittivity of Ch (a) and PItAU_Ch as a function of temperature and frequency.

The registered dielectric loss (ε'' – representing the energy consumed for dipole alignment) presents different shapes for PItAU, Ch and PItAU_Ch (Fig. 8). In the case of PItAU_Ch structure, in the low temperature region, even though there are restricted numbers of dipoles which can rotate within a small angle, the dielectric loss presents slight variations, which attests an increase in the freedom variables justified by the opening of the itaconic anhydride cycle, as well as by the additional physical bonds generated by the Ch presence. Then, with the increase of the temperature, the dielectric loss sharply increases, as the molecular mobility rises and the dipoles absorbing sufficient thermal energy follow the direction of the electric field.

The 3D graph of PItAU_Ch electric permittivity and dielectric loss as a function of frequency and temperature (Fig. 9) confirmed that the main contribution to dielectric relaxation derives from the non-cooperative motion of only the side groups of the ItA comonomer and the functional groups of Ch, which are able of self-assembly processes through physical bonds.

EXPERIMENTAL

1. Materials

All reagents were of analytical purity and used without further purification: 3,9-divinyl-2,4,8,10-tetraoxaspiro[5.5] undecane (U) (purity 98%, Sigma-Aldrich), itaconic anhydride (ITA) (*purity 95%, Aldrich*), 2,2′-Azobis(2-methylpropionitrile) (AIBN) (purity 98%, Sigma-Aldrich), cholesterol (Ch) (from Sigma-Aldrich and Sigma Grade, ≥99%). Also, the solvents 1, 4 dioxane (≥99.0%), diethyl ether (for precipitation) and dimethyl sulfoxide were obtained from Sigma-Aldrich. The water from other experiments was purified using an Ultra Clear TWF UV System.

2. Polymer network synthesis

The synthesis of poly(itaconic anhydride-co-3,9-divinyl-2,4,8,10-tetraoxaspiro[5.5] undecane) (PITAU) copolymer was previously presented. [21] Briefly, the copolymer was synthesized through a radical polymerization process between itaconic anhydride and 3,9-divinyl-2,4,8,10-tetraoxaspiro[5.5] undecane as comonomers, using AIBN as initiator and 1,4-dioxane as solvent. The total monomer concentration was 20% with a ratio between the comonomers of ITA:U = 1:1.5, and the initiator concentration of 0.9% based on the concentration between the comonomers. The continuous polymerization process was conducted under nitrogen atmosphere, at 75°C, in a constant temperature bath, with a stirring rate of 250 rpm, and it was carried out for 17 h. After cooling, the reaction mixture was added dropwise into diethyl ether to precipitate the copolymer which was then washed several times with diethyl ether and dried in a vacuum oven at room temperature and 600 mm HG vacuum for 24 h.

The PITAU_Ch nanogel was prepared by using PITAU (20% solution in dioxane) and Ch (10% solution in dioxane) with a PITAU / Ch ratio of 1/1, 2/1 and 4/1, respectively. The solutions were maintained under nitrogen atmosphere at room temperature for 24 h. Then, the reaction mixtures were added dropwise into diethyl ether for the precipitation of PITAU_Ch, when monodisperse spheres with diameters ranging from 35 nm to 50 nm are obtained. The nanoparticles, washed several times with diethyl ether and dried in a vacuum oven at room temperature and 600 mm HG vacuum for 24 h, were after that ready for characterization.

3. Polymer nanogel structures characterization

3.1. Thermal analysis of the **PItAU_Ch structures** was evaluated in dynamic conditions using STA 449 F1 Jupiter apparatus (Netzsch, Germany) in nitrogen atmosphere at $10^{o}C$ min^{-1} heating rate, in the temperature range 30-650^{o}C. Samples of 10-15 mg were placed in Al_2O_3 crucibles and Al_2O_3 as reference material was used. The gases appearing by the thermal degradation of the samples were analysed using an online connected spectrophotometer FT-IR (Vertex 70) equipped with an external module TGA-IR endowed with

Mercury-Cadmium-Telluride detector and Aëolos QMS 403C mass spectrometer. The acquisition of FT-IR spectra in 3D size was done with OPUS 6.5 software and the spectra were recorded on 600-4000 cm^{-1} interval, at a resolution of 4 cm^{-1}. QMS 403C spectrometer works at 10^{-5} mbar vacuum and electrons impact ionization energy of 70 eV. The data acquisition was achieved in the range m/z=1-300, measurement time 0.5 s for one channel resulting a time/cycle of 150 s.

3.2. Scanning Electron Microscopy

The SEM images of the PItAU_Ch samples in the dry state fixed by means of colloidal copper supports were investigated with a Scanning Electron Microscope, Quanta 200 with EDAX – Elemental Analysis System operating with secondary electrons at 20 kV, under low vacuum mode (60–100 Pa) and LFD detector. The Quanta 200 microscope is equipped with an energy-dispersive X-ray system for qualitative and quantitative analysis. The EDX detector used is the Si detector - EDX silicon-drift detector -which enables rapid determination of elemental compositions and acquisition of compositional maps. The samples were imaged at 10 mm WD (working distance), which is the stage eccentric position and the collection point of the EDX detector, and it is used in conjunction with the LFD (Large Field Detector) detector, at accelerating voltage: 20 KV, low vacuum mode, and uncoated samples.

3.3. Transmission Electron Microscopy

TEM investigations were performed with a Hitachi High-Tech HT7700 electron microscope (Hitachi High-Technologies Corporation, Tokyo, Japan), by using a drop of nanogel solution placed directly on a carbon-coated copper grid and allowed to dry prior to TEM analysis. No staining was made for the sample preparation for this kind of instrument, due to the new high resolution objective lens incorporated in the apparatus. The particle size distribution was evaluated using the UTHSCSA Image Tool Version 3.00 program (UTHSCSA Dental Diagnostic Science, San Antonio, TX, USA). The operated voltage was 30 kV and the current was 36 mA.

3.4. X-ray diffraction analysis

X-ray diffraction analysis of Ch and PItAU_Ch, with PItAU and Ch found in different ratios, was performed on powder samples, equal gravimetric, using the Bruker AXS D8 Advance X-ray diffractometer (Bruker AXS, Madison, USA) by applying 36 kV at 25 mA, Cu anode, ka1 = 1.5406, interval $2\theta = 2 \div 70°$ and $4 \div 40°$, time/step = 0.5 s/step and scanning step size = 0.02, to highlight the modifications brought by the Ch presence into the 3D network structures. The sample holder was rotated to improve the visualization of the particle.

3.5. Circular dichroism (CD) analysis

CD spectra of PItAU_Ch samples were registered on a Chirascan TM CD Spectrometer from Applied Photophysics at 25.0 ±0.2°C in dimethyl sulfoxide (c=50 g/L for PItAU_Ch samples and c=1 g/L for Ch) using quartz cells with a path length of 2.0 mm. Data were collected at the wavelengths from 200 to 600 nm in 1.0 nm increments. Other specifications for the device are: 150W Xe arc, air-cooled light source; wavelength range: 165nm÷1360nm; stray light: <3ppm at 200nm; baseline stability: ±0.02 mo /hr; CD full scale: ±6000 mo; CD resolution: better than 0.0001mo in 6000mo; kinetic modes: linear timebase, split-linear time bases, logarithmic time base; detection modes: circular dichroism; cell holder with Peltier temperature control.

3.6. Dielectric spectroscopy

Complex dielectric permittivity measurements of PItAU_Ch samples were performed using the Novocontrol Dielectric Spectrometer (GmbH Germany), CONCEPT 40 in the range of frequency (1-10^6 Hz) and temperature (-150°C - 120°C), at the amplitude of applied voltage of 1 V, in nitrogen atmosphere avoiding water absorption. Novocontrol QuatroCryosystem device was used in order to control the temperature with 0.1°C stability. The samples were prepared as pellets with 0.6 mm thick and then sandwiched between two gold coated plate electrodes.

CONCLUSIONS

The new characteristics of the PItAU_Ch nanogel structure compared with the PItAU starting copolymer are put into evidence. Thus, increased thermal stability is registered and justified by the new physical bonds and self-assembled structure of PItAU_Ch, which is generated by the Ch presence. TEM images, reflecting the spherical morphology of the PItAU_Ch nanogels, evidence also the connection between the Ch content and the cholesterol capacity to induce self-assembly in the new synthesised nanoparticles. The investigations performed on the PItAU_Ch by circular dichroism and dielectric spectroscopy confirm the Ch covalent bonded resulted after opening the itaconic anhydride cycle, as differences between the behaviour of PItAU copolymer and PItAU_Ch are registered.

REFERENCES

1. F. Fages, “Low molecular mass gelators; design, self-assembly, function”, Springer, 2005.
2. M. Žinic, F. Vögtle and F. Fages, “Cholesterol-based gelators” in “Low molecular mass gelators; design, self-assembly, function”, F. Fages (Ed.), Springer-Verlag, Berlin, Heidelberg, 2005, p. 39–76.
3. T.D. James, H. Kawabata, R. Ludwig, K. Murata and S. Shinkai, *Tetrahedron*, **1995**, *51*, 555-566.
4. X.-F. Liu, X.-X. Xu, Q. Li, J.-S. Hu, L.-Q. Yang and Q.-F. Chen, *Liq. Cryst*., **2017**, *44*, 1356-1364.
5. P.-L. Champagne, D. Ester, S. Aldosari, V.E. Williams and C.-C. Ling, *Liq. Cryst*., **2017**
6. J. Xiong, X. Lin, H. Guo, F. Yang and J. Lai, *Liq. Cryst*., **2017**, *45*, 362-369.
7. F. van de Manakker, M. van der Pot, T. Vermonden, C.F. van Nostrum and W.E. Hennink, *Macromolecules*, **2008**, *41*, 1766-1773.
8. J. Yan, J. Liu, P. Jing, C. Xu, J. Wu, D. Gao and Y. Fang, *Soft Matter*, **2012**, ***8***, 11697-11703 .
9. M. Xue, K. Liu, J. Peng, Q. Zhang and Y. Fang, *J. Colloid Interface Sci.,* **2008**, *327*, 94–101.
10. D. Gao, M. Xue, J. Peng, J. Liu, N. Yan, P. He and Y. Fang, *Tetrahedron*, **2010**, *66*, 2961–2968.
11. Y. Ren, B. Wang and X. Zhang, *Beilstein J. Org. Chem*., **2015**, *11*, 1089–1095.

12. Z. Matharu, G. Sumana, S.K. Arya, S.P. Singh, V. Gupta and B.D. Malhotra, *Langmuir*, **2007**, *23*, 13188–13192.
13. K. Kim, C. Kim, Y. Byun, *Langmuir*, **2001**, *17*, 5066-5070.
14. L. Lu and R.G. Weiss, *Langmuir*, **1995**, *11*, 3630–3632.
15. C.D. Varganici, A. Durdureanu-Angheluta, D. Rosu, M. Pinteala, B. C. Simionescu; *J. Anal. Applied Pyrolysis,* **2012,** *96*, 63-68.
16. P. Wallimann, T. Marti, A. Furer and F. Diederich, *Chem. Rev.* **1997**, *97*, 1567–1608.
17. H. A. Klok, J. J. Hwang, S. N. Lyer and S. I. Stupp, *Macromolecules*, **2002**, *35*, 746–759.
18. A. P. Chiriac, L. E. Nita and M. T. Nistor, *J. Polym. Sci., Part A: Polym. Chem.*, **2011**, *49*, 1543–1551.
19. L. E. Nita, A. P. Chiriac, M. T. Nistor and I. Neamtu, *Rev. Roum. Chim.*, **2013**, *58*, 137-143.
20. A. P. Chiriac, L. E. Nita, N. Tudorachi, I. Neamtu, V. Balan and L. Tartau, *Mater. Sci. Eng., C*, **2015**, *50*, 348–357.
21. A. Diaconu, A.P. Chiriac, L.E. Nita, N. Tudorachi, I. Neamtu, C. Vasile and M. Pinteala, *Des. Monomers Polym*., **2015**, *18*, 780–788.
22. L. E. Nita, A. P. Chiriac, A. Diaconu, N. Tudorachi and L. Mititelu-Tartau, *Int. J. Pharm*., **2016**, *515*, 165-175.
23. A. P. Chiriac, L. E. Nita, A. Diaconu, M. Bercea, N. Tudorachi, D. Pamfil, L. Mititelu-Tartau, *Int. J. Biol. Macromol*., **2017**, *98*, 407-418.
24. A. Diaconu, L.E. Nita, M. Bercea, A.P. Chiriac, A.G. Rusu and D. Rusu, *Biochem. Eng. J*., **2017**, *125*, 135-143.
25. A. P. Chiriac, L. E. Nita, A. Diaconu, A. G. Rusu and I. Neamtu; Smart Gel Structures Based on a New Macromolecular Compound and Low Molecular Mass Gelators; *The 9-th International Symposium* "Molecular Mobility and Order in Polymer Systems", Saint Petersburg, Peterhof, June 19-23, 2017; http://www.mmops2017.com/
26. A. P. Chiriac, L. E. Nita, A. Diaconu, A. G. Rusu and I. Neamtu; Polymeric networks based on a Copolymer Containing Pendant Spiroacetal Moieties and low molecular mass gelators; Baltic Conference Series; www.vbripress.com/bcs17winter, DOI: 10.5185/bcs17winter.2017
27. A. P. Chiriac, L. E. Nita, A. Diaconu, A. G. Rusu, I. Neamtu and D. Rusu, *Curr. Appl. Polym. Sci*., **2017**, *2*, 1-7.
28. Information on http:// webbook.nist.gov/ chemistry/name-ser.html .
29. Information on TGA-IR user manual, Bruker].
30. A. A. Christy, M. I. Lian and G. W. Francis, *Food Chem*., **2011**, *124*, 1466–1472.
31. C. D. Varganici, A. Durdureanu-Angheluta, D. Rosu, M. Pinteala, B. C. Simionescu, *Journal of Analytical and Applied Pyrolysis*, **2012,** *96*, 63-68
32. X. H. Weerakoon, A. Navaratne, S. Ranasinghe, R. Sivakanesan, K. B. Galketiya and S. Rosairo**,** *Plos One*, **2015**.
33. J. Zbytovská, M. A. Kiselev, S. S. Funari, V. M. Garamus, S. Wartewig, K. Palát and R. Neubert, *Colloids Surf. A*, **2008**, *328*, 90–99.
34. H. Yao, E. Wynendaele, X. Xu, A. Kosgei and B. De Spiegeleer, *J. Pharm. Biomed. Anal*., **2018**, *147*, 50–64.
35. A. Bonvicini, L. Guilhaudis, V. Tognetti, D. Desmaele, N. Sauvonnet,H. Oulyadia and L. Joubert, *Phys. Chem. Chem. Phys*., **2018**, *20*, 5274-5284.
36. Q. Ye ,D. Zhu , H. Zhang, X. Lu and Q. Lu, *J. Mater. Chem. C*, **2015**, ***3***, 6997-7003.
37. A. P. Chiriac, L. E. Nita and M. T. Nistor, J. Nanopart. Res., **2011**, *13*, 6953–6962.
38. A. P. Chiriac, V. Balan, M. Asandulesa, E. Butnaru, N. Tudorachi, E. Stoleru, L. E. Nita, I. Neamtu and A. Diaconu, *Mater. Chem. Phys.,* **2016**, *180*, 291- 300.